Simplified methods and a posteriori error estimation for the homogenization of representative volume elements (RVE)

Nicolas Moës, John Tinsley Oden, Kumar Vemaganti, Jean-François Remacle

Simplified methods and a posteriori error estimation for the homogenization of representative volume elements (RVE)

Nicolas Moës[a], J. Tinsley Oden,[a,*], Kumar Vemaganti[a], Jean-François Remacle[b]

[a]*The Texas Institute for Computational and Applied Mathematics, The University of Texas at Austin, Austin, TX 78712, USA*

[b]*Ecole polytechnique de Montréal, Département de génie mécanique, Campus de l'Université de Montréal, 13T 1J4 Montréal, Québec, Canada*

Homogenization techniques usually rely on solving a boundary value problem on the representative element volume (RVE). This problem is generally complex to solve when the micro-structure is realistic, especially in three dimensions. In this paper, we develop two simplified methods providing approximate micro-fields over the RVE. These fields yield upper *and* lower bounds to the exact homogenized property. The a posteriori estimation of the modeling error introduced by the simplified methods is thus straightforward. Both simplified methods are based on a two-scale strategy. The RVE is decomposed into subdomains over which the solution is sought as a smooth part (meso-scale) plus a correction (micro-scale). The correction is expressed in terms of smooth part through a prolongation operator. This operation is performed independently on each subdomain and is thus readily parallelizable. Then, the smooth part of the solution is obtained by solving a 'meso' problem involving all the subdomains. In the numerical experiments, we consider 2-D linear scalar diffusion problems with periodic boundary conditions on the RVE. The RVE is made of a two-phase material consisting of a matrix in which circular or elliptical inclusions are distributed randomly. Numerical examples arecomputed in a parallel computation done on a cluster of 16 Intel P.C.

1. Introduction

We are interested in the linear multi-scale problems of the type suggested in the sketch in Fig. 1. The structure (macro-scale) is assumed to be obtained by the periodic repetition of the representative volume element (meso-scale). The RVE is considered to be complex so that it may decomposed into micro-scale entities. Roughly speaking, the meso-scale involves the inclusions interactions whereas the micro-scale involves the inclusion-matrix interactions.

The size of the RVE is assumed to be small compared to the macro-scale so that the 'asymptotic' homogenization theory applies [1]. The homogenized properties are obtained by solving a periodic boundary value problems on the RVE. This problem is difficult when the micro-structure is complex so that simplified techniques have been proposed in the literature [2–4].

In this paper, we introduce a new method in which the solution over the RVE is modeled as the sum of two components: meso-scale and micro-scale components. One of the main concerns in the development of the method is to be able to obtain an a posteriori estimate of the modeling error introduced. In this sense, the present work is related to previous work on hierarchical modeling of heterogeneous bodies by Oden et al. [5–7]. We also note that a similar approach to homogenization techniques for porous media is being developed by Arbogast [8] using mixed finite element techniques.

* Corresponding author.

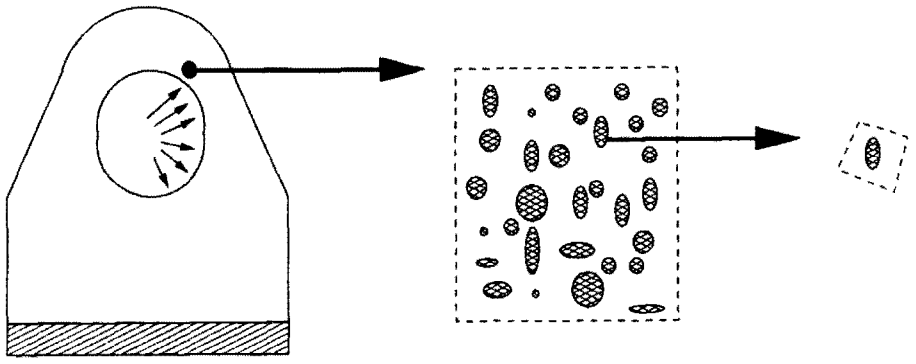

Fig. 1. The different scales associated to the model problem.

The proposed approach consists of five steps:

(1) The RVE is decomposed into subdomains whose sizes are approximately the size of the micro features in the RVE, Fig. 3.
(2) On each subdomain, the solution is expressed as the sum of a meso-scale and a micro-scale component.
(3) Still on each subdomain, the micro-scale part of the solution is expressed in terms of the meso-scale part through a boundary value problem (homogenization step).
(4) The subdomains are assembled to define a meso-scale problem to be solved on the RVE.
(5) The meso-scale being known, one recovers the micro-part of the solution on each subdomain using the results of the third step above (localization step).

By properly choosing the type of boundary conditions used in step 3 and the way the subdomains are assembled to create the meso-problem in step 4, it is possible to obtain lower and upper bounds to the exact homogenized properties of the RVE. The modeling error is thus easy to estimate.

Concerning the practical implementation of the methods, parallel computing resources are used, especially for steps 3 and 5. Also, for flexibility, finite elements are used in step 3.

The plan of the paper is as follows. In Section 2, the problem to be solved on the RVE is detailed, first in the strong form and then in two equivalent variational forms: primal and hybrid. Section 3 introduces the two simplified methods to model the reference problem and the bounds on the homogenized property are derived. Then, Section 4 is devoted to the practical case of the use of the finite-element method to solve the boundary value problems appearing in the simplified strategies. Numerical experiments are carried out in Section 5 and the major points of the paper are summarized in the conclusion.

2. Description of the problem

Scalars will be italic and vectors bold. For instance, the temperature will be denoted by u and the heat flux and the temperature gradient will be denoted by $\boldsymbol{\sigma}$ and $\boldsymbol{\epsilon}$, respectively. More complex operators will be uppercase (e.g. E for the conductivity tensor). We consider a cell $\Omega = (-1, 1)^n$, $n = 1, 2, 3$, occupied by a heterogeneous linearly-conductive material, Fig. 2. We assume that Ω contains no holes or cracks. We denote by $\partial\Omega$ the boundary of Ω and $\boldsymbol{n}$ the outward unit normal along $\partial\Omega$. We define $\partial\Omega_{\#}$ as the set of pairs of point facing each other on the boundary of Ω:

$$\partial\Omega_{\#} = \{(\boldsymbol{x}, \boldsymbol{x}') : \boldsymbol{x},\ \boldsymbol{x}' \in \partial\Omega,\ \boldsymbol{x} \neq \boldsymbol{x}',\ (\boldsymbol{x} - \boldsymbol{x}') \wedge \boldsymbol{n} = 0;\ \boldsymbol{n} \text{ outward normal at } \boldsymbol{x}\}$$

The average over Ω of a field a defined on Ω will be denoted by $\langle a \rangle$.

Assuming periodic boundary conditions, the homogenization problem to be solved on Ω is to find a triple $(u, \boldsymbol{\epsilon}, \boldsymbol{\sigma})$ such that the temperature constraints, the conservation law and the constitutive law hold:

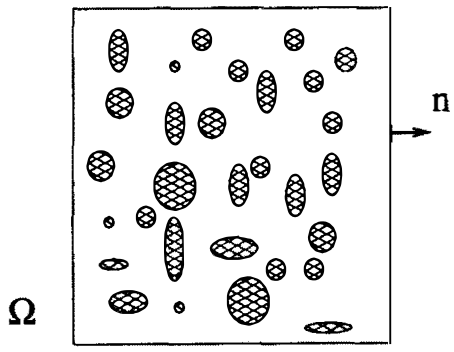

Fig. 2. Geometry of the RVE problem.

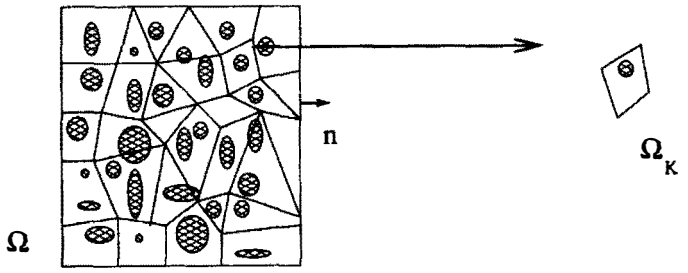

Fig. 3. Domain decomposition.

$$\left.\begin{array}{lll} \boldsymbol{\epsilon}=\bar{\boldsymbol{\epsilon}}+\nabla u & \text{on } \Omega, & \langle\boldsymbol{\epsilon}\rangle=\bar{\boldsymbol{\epsilon}} \\ \operatorname{div}\boldsymbol{\sigma}=0 & \text{on } \Omega & \langle\boldsymbol{\sigma}\rangle=\bar{\boldsymbol{\sigma}} \\ u(\boldsymbol{x})=u(\boldsymbol{x}') & \forall\,(\boldsymbol{x},\boldsymbol{x}')\in\partial\Omega_{\#} & \\ \boldsymbol{\sigma}(\boldsymbol{x})\cdot\boldsymbol{n}=-\boldsymbol{\sigma}(\boldsymbol{x}')\cdot\boldsymbol{n}' & \forall\,(\boldsymbol{x},\boldsymbol{x}')\in\partial\Omega_{\#} & \\ \boldsymbol{\sigma}=E\boldsymbol{\epsilon} & \text{on } \Omega & \end{array}\right\} \tag{1}$$

Either $\bar{\boldsymbol{\epsilon}}$ or $\bar{\boldsymbol{\sigma}}$ is given. In the sequel we shall consider $\bar{\boldsymbol{\epsilon}}$ as given. The conductivity tensor E is a function of position $\boldsymbol{x}$ i.e. $E=E(\boldsymbol{x})\in L^{\infty}(\Omega)^{n\times n}$ and E is symmetric and elliptic; i.e. for a.e. $\boldsymbol{x}\in\Omega$, there are constants α_0, $\alpha_1>0$, such that $\alpha_0\boldsymbol{a}^t\boldsymbol{a}\leq\boldsymbol{a}^tE(\boldsymbol{x})\boldsymbol{a}\leq\alpha_1\boldsymbol{a}^t\boldsymbol{a}$ for any $\boldsymbol{a}\in\mathbb{R}^n$. Problem (1) corresponds to a heat transfer homogenization procedure problem if $-\boldsymbol{\sigma}$ is understood as the heat flux.

REMARK. Let $(\boldsymbol{\sigma}, \boldsymbol{\epsilon})$ be a heat flux, temperature gradient pair satisfying the first four equations of the problem (1). This pair satisfies Hill's macrohomogeneity equality (see [9]):

$$\langle\boldsymbol{\sigma}\cdot\boldsymbol{\epsilon}\rangle=\bar{\boldsymbol{\sigma}}\cdot\bar{\boldsymbol{\epsilon}} \tag{2}$$

This equality expresses the equality of virtual work between the microscopic scale and the macroscopic scale.

The remainder of this Section is devoted to the description of two variational formulations associated to the strong form (1). The first is the classical primal formulation which corresponds to the minimization of the potential energy. The second is the primal hybrid formulation which involves a saddle-point problem.

2.1. Primal formulation

Using the convenient notation, $\bar{u}=\bar{\boldsymbol{\epsilon}}\cdot\boldsymbol{x}$, and eliminating $\boldsymbol{\epsilon}$ and $\boldsymbol{\sigma}$ in (1), we obtain a formulation involving only the temperature field:

$$\left.\begin{array}{ll} \operatorname{div}(E\nabla(u+\bar{u}))=0 & \\ u(x)=u(x') & \forall\,(x,x')\in\partial\Omega_{\#} \\ ((E\nabla(u+\bar{u}))\cdot n')\,|_{x}+((E\nabla(u+\bar{u}))\cdot n')|_{x'}=0 & \forall\,(x,x')\in\partial\Omega_{\#} \end{array}\right\} \tag{3}$$

A weak formulation of problem (3) is to find $u\in\mathcal{V}_{\#}$ such that

$$B(u+\bar{u},v)=0 \quad \forall\, v\in\mathcal{V}_{\#} \tag{4}$$

where

$$\mathcal{V}_{\#}=\{v\in H^{1}(\Omega):\, v(x)=v(x')\ \forall\,(x,x')\in\partial\Omega_{\#}\}, \qquad B(u,v)=\int_{\Omega} E\nabla u\cdot\nabla v\,\mathrm{d}x$$

Owing to the assumed properties of E, $B(\cdot,\cdot)$ is symmetric coercive and induces the energy norm on $\mathcal{V}$:

$$\|v\|_{E(\Omega)}=\{B(v,v)\}^{1/2} \tag{5}$$

Problem (4) possesses a unique solution for given $\bar{u}$ and, as is well known, this solution also minimizes the total potential energy $J(v)=\frac{1}{2}B(v+\bar{u},\, v+\bar{u})$

$$J(u)=\inf_{v\in\mathcal{V}_{\#}} J(v) \tag{6}$$

REMARK. The minimization problem (6) defines the solution u as a function of the data $\bar{\boldsymbol{\epsilon}}$: $u=u(\bar{\boldsymbol{\epsilon}})$. There exists a linear symmetric and elliptic operator E^{HOM} such that

$$J(u(\bar{\boldsymbol{\epsilon}}))=\frac{1}{2}E^{\mathrm{HOM}}\bar{\boldsymbol{\epsilon}}\cdot\bar{\boldsymbol{\epsilon}}, \qquad \forall\,\bar{\boldsymbol{\epsilon}}\in\mathbb{R}^{n\times n} \tag{7}$$

and the homogenized constitutive relation associated to the RVE is $\bar{\boldsymbol{\sigma}}=E^{\mathrm{HOM}}\bar{\boldsymbol{\epsilon}}$ (see [1]).

2.2. Primal hybrid formulation

This type of formulation has been introduced in [10,11] and mathematically studied in [12,13]. We need a partition $\mathcal{P}$ of the domain Ω into N subdomains Ω_k, $1\leqslant k\leqslant N$:

$$\bar{\Omega}=\cup_{k=1}^{N}\bar{\Omega}_k, \qquad \Omega_k\cap\Omega_l=\emptyset, \qquad k\neq l \tag{8}$$

For any $\Omega_k\subset\Omega$, we denote by $\partial\Omega_k$ the boundary and $\boldsymbol{n}_k$ the unit outward normal along Ω_k. $\partial\Omega_k$ is assumed to be Lipschitz. Each Ω_k is assumed to be the image of a master element $\hat{\Omega}$ under an affine invertible map F_k, $1\leqslant k\leqslant N$. We need three spaces: the space $\mathcal{W}$ of non-conforming temperatures

$$\mathcal{W}=\{w\in L^{2}(\Omega);\, w_k\in H^{1}(\Omega_k),\ 1\leqslant k\leqslant N\} \tag{9}$$

where w_k is the restriction of w to Ω_k, the space $\mathcal{M}$ of continuous heat fluxes across the boundary of the subdomains

$$\mathcal{M}=\left\{\mu\in\prod_{k=1}^{N}H^{-1/2}(\partial\Omega_k);\ \exists\,\tau\in H(\mathrm{div};\Omega)\ \text{s.t.}\ \tau\cdot\boldsymbol{n}_k=\mu\ \text{ on }\partial\Omega_k,\ 1\leqslant k\leqslant N\right\}$$

and the subspace $\mathcal{M}_{\#}\subset\mathcal{M}$ of anti-periodic fluxes on $\partial\Omega$

$$\mathcal{M}_{\#}=\{\mu\in\mathcal{M}:\,\mu(x)+\mu(x')=0\ \forall\,(x,x')\in\partial\Omega_{\#}\} \tag{10}$$

The primal hybrid formulation is to find a pair $(w,\lambda)\in\mathcal{W}\times\mathcal{M}_{\#}$ such that

$$\begin{cases} A(w+\bar{u},v)+C(v,\lambda)=0 & \forall\, v\in\mathcal{W} \\ C(w,\mu)=0 & \forall\,\mu\in\mathcal{M}_{\#} \end{cases} \tag{11}$$

where

$$A(w, v)=\sum_{k=1}^{N}\int_{\Omega_k} E\nabla w\cdot\nabla v\ \mathrm{d}x, \qquad C(v, \mu)=-\sum_{k=1}^{N}\int_{\partial\Omega_k}\mu v\ \mathrm{d}s \tag{12}$$

Here '$\int_{\partial\Omega_k}\mu v\ \mathrm{d}s$' denotes the duality pairing on $H^{-1/2}(\partial\Omega_k)$ and $H^{1/2}(\partial\Omega_k)$. Using the results in [12], one can show that

- problem (11) has a unique solution (w, λ); the solution w belongs to $\mathcal{V}_{\#}$ and is equal to the solution u of (4);
- problem (11) is equivalent to the saddle point problem

$$L(w, \lambda)=\inf_{v\in\mathcal{W}}\sup_{\mu\in\mathcal{M}_{\#}} L(v, \mu)=\sup_{\mu\in\mathcal{M}_{\#}}\inf_{v\in\mathcal{W}} L(v, \mu) \tag{13}$$

  where

$$L(v, \mu)=J(v)+C(v, \mu) \tag{14}$$

- the solution (w, λ) to (11) and the solution u to (4) satisfy the equality

$$L(w, \lambda)=J(u) \tag{15}$$

It is clear that if w is sufficiently smooth, the multipliers λ are the boundary fluxes $\lambda=(E\nabla(w+\bar{u}))\cdot\boldsymbol{n}$ on subdomain boundaries.

3. Two-scale modeling strategy

The goal is to replace the spaces $\mathcal{V}_{\#}$ and $\mathcal{M}_{\#}$ by the subspaces $\tilde{\mathcal{V}}_{\#}\subset\mathcal{V}_{\#}$ and $\tilde{\mathcal{M}}_{\#}\subset\mathcal{M}_{\#}$ so that the approximate solutions $\tilde{u}$ and $(\tilde{w}, \tilde{\lambda})$ defined by

$$J(\tilde{u})=\inf_{v\in\tilde{\mathcal{V}}_{\#}} J(v) \tag{16}$$

$$L(\tilde{w}, \tilde{\lambda})=\inf_{v\in\mathcal{W}}\sup_{\mu\in\tilde{\mathcal{M}}_{\#}} L(v, \mu) \tag{17}$$

yield upper and lower bounds to the exact energy

$$L(\tilde{w}, \tilde{\lambda})\leqslant L(w, \lambda)=J(u)\leqslant J(\tilde{u}) \tag{18}$$

and thus upper and lower bounds to the homogenized properties owing to (7).

The construction of the subspaces uses a two-scale representation of the solution: a meso-scale component will take into account the interaction between the subdomains and a micro-scale component will depend on the micro-structure of each subdomain. In the sequel, the superscript 'M' shall denote meso-scale related quantities and the superscript 'm' the related micro-scale quantities.

3.1. Upper bound

We particularize the partition $\mathcal{P}$ by assuming that it is a triangulation of the set $\overline{\Omega}$ and that each subdomain Ω_k is a polyhedron. As indicated earlier, each $\Omega_k\subset\Omega$ is the image of $\hat{\Omega}$ through an affine invertible mapping F_k. The boundary of each $\hat{\Omega}$ will be denoted by $\partial\hat{\Omega}$. The approximate temperature field $\tilde{u}$ is sought as the sum of a smooth conforming temperature field u^{M} which is polynomial over each subdomain and a 'rough' correction field u^{m} having a zero value on the boundary of each subdomain. More precisely, on each subdomain Ω_k, we define the spaces $\mathcal{V}_k^{\mathrm{M}}$ and $\mathcal{V}_k^{\mathrm{m}}$ such that

$$\mathcal{V}_k^{\mathrm{M}} = \left\{ v \in H^1(\Omega_k) : v = \hat{v} \circ F_k^{-1},\ \hat{v} \in P_p(\hat{\Omega}) \right\} \tag{19}$$

$$\mathcal{V}_k^{\mathrm{m}} = \left\{ v \in H^1(\Omega_k) : v_k = 0 \text{ on } \partial\Omega_k \right\} \tag{20}$$

where $P_p(\hat{\Omega})$, $p \geq 1$, is the space of polynomials of degree $\leq p$ in the n variables $x_1, \ldots, x_n$ defined over $\hat{\Omega}$. We also define the corresponding global spaces $\mathcal{V}_{\#}^{\mathrm{M}}$ and $\mathcal{V}_{\#}^{\mathrm{m}}$ and the space of approximation $\tilde{\mathcal{V}}_{\#}$

$$\mathcal{V}_{\#}^{\mathrm{M}} = \left\{ v \in \mathcal{V}_{\#} : v_k \in \mathcal{V}_k^{\mathrm{M}},\ 1 \leq k \leq N \right\} \cap C^0(\Omega) \tag{21}$$

$$\mathcal{V}_{\#}^{\mathrm{m}} = \left\{ v \in \mathcal{V}_{\#} : v_k \in \mathcal{V}_k^{\mathrm{m}},\ 1 \leq k \leq N \right\} \tag{22}$$

$$\tilde{\mathcal{V}}_{\#} = \left\{ v = v^{\mathrm{M}} + v^{\mathrm{m}} : v^{\mathrm{M}} \in \mathcal{V}_{\#}^{\mathrm{M}},\ v^{\mathrm{m}} \in \mathcal{V}_{\#}^{\mathrm{m}} \right\} = \mathcal{V}_{\#}^{\mathrm{M}} + \mathcal{V}_{\#}^{\mathrm{m}} \tag{23}$$

It is not difficult to show that the inclusion $\tilde{\mathcal{V}}_{\#} \subset \mathcal{V}_{\#}$ holds.

Let us now detail the practical treatment of (16). Using the decomposition (23), we obtain

$$\inf_{v \in \tilde{\mathcal{V}}_{\#}} J(v) = \inf_{v^{\mathrm{M}} \in \mathcal{V}_{\#}^{\mathrm{M}}} \inf_{v^{\mathrm{m}} \in \mathcal{V}_{\#}^{\mathrm{m}}} J(v^{\mathrm{M}} + v^{\mathrm{m}}) \tag{24}$$

The second infimum may be split into a sum of independent infima:

$$\inf_{v^{\mathrm{m}} \in \mathcal{V}_{\#}^{\mathrm{m}}} J(v^{\mathrm{M}} + v^{\mathrm{m}}) = \sum_{k=1}^{N} \inf_{v_k^{\mathrm{m}} \in \mathcal{V}_k^{\mathrm{m}}} J_k(v_k^{\mathrm{M}} + v_k^{\mathrm{m}}) \tag{25}$$

where

$$J_k(v) = \frac{1}{2} B_k(v + \bar{u}_k, v + \bar{u}_k), \quad B_k(v, v) = \int_{\Omega_k} E\, \nabla v \cdot \nabla v \, \mathrm{d}x \tag{26}$$

In the minimization problem (25), v_k^{M} is considered as an imposed parametric function belonging to $\mathcal{V}_k^{\mathrm{M}}$. For each subdomain, the infimum is given by $v_k^{\mathrm{m}} = u_k^{\mathrm{m}}(v_k^{\mathrm{M}}) + \bar{u}_k^{\mathrm{m}}$ where $u_k^{\mathrm{m}}(v_k^{\mathrm{M}})$ is defined for all $v_k^{\mathrm{M}} \in \mathcal{V}_k^{\mathrm{M}}$ by the problem

$$u_k^{\mathrm{m}}(v_k^{\mathrm{M}}) \in \mathcal{V}_k^{\mathrm{m}} : B_k(v_k^{\mathrm{M}} + u_k^{\mathrm{m}}(v_k^{\mathrm{M}}), v_k^{\mathrm{m}}) = 0 \quad \forall\, v_k^{\mathrm{m}} \in \mathcal{V}_k^{\mathrm{m}} \tag{27}$$

and $\bar{u}_k^{\mathrm{m}}$ is defined by the problem

$$\bar{u}_k^{\mathrm{m}} \in \mathcal{V}_k^{\mathrm{m}} : B_k(\bar{u}_k^{\mathrm{m}} + \bar{u}_k, v_k^{\mathrm{m}}) = 0 \quad \forall\, v_k^{\mathrm{m}} \in \mathcal{V}_k^{\mathrm{m}} \tag{28}$$

We can introduce the local homogenized potential by

$$J_k^{\mathrm{hom}}(v_k^{\mathrm{M}}) = J_k(v_k^{\mathrm{M}} + u_k^{\mathrm{m}}(v_k^{\mathrm{M}}) + \bar{u}_k^{\mathrm{m}}) \tag{29}$$

Noting that $\mathcal{V}_{\#}^{\mathrm{M}} \subset \prod_{k=1}^{N} \mathcal{V}_k^{\mathrm{M}}$, the minimization problem (16) takes the form

$$J(\tilde{u}) = J^{\mathrm{hom}}(u^{\mathrm{M}}) = \inf_{v^{\mathrm{M}} \in \mathcal{V}_{\#}^{\mathrm{M}}} J^{\mathrm{hom}}(v^{\mathrm{M}}) \quad \text{where} \quad J^{\mathrm{hom}}(v^{\mathrm{M}}) = \sum_{k=1}^{N} J_k^{\mathrm{hom}}(v_k^{\mathrm{M}}) \tag{30}$$

3.2. Lower bound

We need to build the subspace $\tilde{\mathcal{M}}_{\#} \subset \mathcal{M}_{\#}$ where $\mathcal{M}_{\#}$ is recalled below:

$$\mathcal{M}_{\#} = \left\{ \mu \in \mathcal{M} : \mu(\boldsymbol{x}) + \mu(\boldsymbol{x}') = 0 \ \forall\, (\boldsymbol{x}, \boldsymbol{x}') \in \partial\Omega_{\#} \right\}$$

$$\mathcal{M} = \left\{ \mu \in \prod_{k=1}^{N} H^{-1/2}(\partial\Omega_k);\ \exists \boldsymbol{\tau} \in H(\mathrm{div};\, \Omega) \text{ s.t. } \boldsymbol{\tau} \cdot \mathbf{n}_k = \mu \text{ on } \partial\Omega_k,\ 1 \leq k \leq N \right\}$$

This is done using the ideas developed for hybrid finite elements, (see [12,13]). First, we design a subspace $\mathcal{M}_k^{\mathrm{M}} \subset H^{-1/2}(\partial\Omega_k)$. We denote $S_m(\partial\hat{\Omega})$ the set of all functions defined over $\partial\hat{\Omega}$ whose restrictions to any $(n-1)$-dimensional face $\hat{\Omega}'$ of $\partial\hat{\Omega}$ are polynomials of degree $\leq m$.

$$\mathcal{M}_k^{\mathrm{M}} = \left\{\mu \in L^2(\partial\Omega_k):\ \mu = \hat{\mu} \circ F_k^{-1};\ \hat{\mu} \in S_m(\partial\hat{\Omega})\right\} \tag{31}$$

Then, we build $\tilde{\mathcal{M}}_{\#} = \mathcal{M}_{\#}^{\mathrm{M}} \subset \mathcal{M}_{\#}$ as

$$\mathcal{M}_{\#}^{\mathrm{M}} = \left\{\mu \in \mathcal{M}^{\mathrm{M}}:\ \mu(\boldsymbol{x}) + \mu(\boldsymbol{x}') = 0\ \forall\, (\boldsymbol{x}, \boldsymbol{x}') \in \partial\Omega_{\#}\right\} \tag{32}$$

$$\mathcal{M}^{\mathrm{M}} = \left\{ \mu \in \prod_{k=1}^{N} \mathcal{M}_k^{\mathrm{M}};\ \mu|_{\partial\Omega_k} + \mu|_{\partial\Omega_l} = 0 \text{ on } \Omega_k \cap \Omega_l, \quad \forall\, \overline{\Omega_k},\ \overline{\Omega_l} \text{ s.t. } \overline{\Omega_k} \cap \overline{\Omega_l} \neq \emptyset \right\} \tag{33}$$

The saddle-point problem (3.2) now reads

$$L(\tilde{w},\ \lambda^{\mathrm{M}}) = \inf_{v \in \mathcal{W}} \sup_{\mu^{\mathrm{M}} \in \mathcal{M}_{\#}^{\mathrm{M}}} L(v,\ \mu^{\mathrm{M}}) \tag{34}$$

This problem may be proved to be well posed using the results in [12,13].

For the implementation of the saddle-point problem (34), it is useful to decompose the space $\mathcal{W}$ into meso and micro components: $\mathcal{W}^{\mathrm{M}}$ and $\mathcal{W}^{\mathrm{m}}$. The decomposition is performed independently in each subdomain and must satisfy the direct sum relation

$$\mathcal{W}_k = \mathcal{W}_k^{\mathrm{M}} \oplus \mathcal{W}_k^{\mathrm{m}} \tag{35}$$

which must be understood in the following *algebraic* sense

$$\begin{cases} \mathcal{W}_k^{\mathrm{M}} \cap \mathcal{W}_k^{\mathrm{m}} = \{0\} \\ \forall\, v^{\mathrm{M}} \in \mathcal{W}_k^{\mathrm{M}},\ v^{\mathrm{m}} \in \mathcal{W}_k^{\mathrm{m}}:\ v^{\mathrm{M}} + v^{\mathrm{m}} \in \mathcal{W}_k \\ \forall\, v \in \mathcal{W}_k:\ \exists! v^{\mathrm{M}} \in \mathcal{W}_k^{\mathrm{M}},\ v^{\mathrm{m}} \in \mathcal{W}_k^{\mathrm{m}}:\ v = v^{\mathrm{M}} + v^{\mathrm{m}} \end{cases} \tag{36}$$

EXAMPLE. As an example of such a decomposition, we may take $\mathcal{W}_k^{\mathrm{M}} = \mathcal{V}_k^{\mathrm{M}}$ defined previously equation (19) and $\mathcal{W}_k^{\mathrm{m}}$ as the orthogonal complement in the $H^1(\Omega_k)$ inner product, all the constant modes being excluded:

$$\mathcal{W}_k^{\mathrm{m}} = \left\{v \in \mathcal{W}_k:\ \int_{\Omega_k} \nabla v \cdot \nabla v^{\mathrm{M}}\, \mathrm{d}x = 0 \quad \forall\, v^{\mathrm{M}} \in \mathcal{W}_k^{\mathrm{M}},\ \int_{\Omega_k} v\, \mathrm{d}x = 0\right\} \tag{37}$$

Note that for a given choice of $\mathcal{W}_k^{\mathrm{M}}$, the choice of $\mathcal{W}_k^{\mathrm{m}}$ satisfying the conditions (36) is not unique. The choice in the example above is particular since orthogonality is not required.

The local decomposition (35) leads to the global decomposition $\mathcal{W} = \mathcal{W}^{\mathrm{M}} \oplus \mathcal{W}^{\mathrm{m}}$ where

$$\mathcal{W}^{\mathrm{M}} = \left\{v \in L^2(\Omega);\ v_k \in \mathcal{W}_k^{\mathrm{M}},\ 1 \leqslant k \leqslant N\right\} \tag{38}$$

$$\mathcal{W}^{\mathrm{m}} = \left\{v \in L^2(\Omega);\ v_k \in \mathcal{W}_k^{\mathrm{m}},\ 1 \leqslant k \leqslant N\right\} \tag{39}$$

Introducing the decomposition of $\mathcal{W}$ in the saddle-point problem (34), we obtain

$$\begin{aligned} &\inf_{v \in \mathcal{W}} \sup_{\mu^{\mathrm{M}} \in \mathcal{M}_{\#}^{\mathrm{M}}} L(v,\ \mu^{\mathrm{M}}) = \sup_{\mu^{\mathrm{M}} \in \mathcal{M}_{\#}^{\mathrm{M}}} \inf_{v \in \mathcal{W}} L(v,\ \mu^{\mathrm{M}}) \\ &= \sup_{\mu^{\mathrm{M}} \in \mathcal{M}_{\#}^{\mathrm{M}}} \inf_{v^{\mathrm{M}} \in \mathcal{W}^{\mathrm{M}}} \inf_{v^{\mathrm{m}} \in \mathcal{W}^{\mathrm{m}}} L(v^{\mathrm{M}} + v^{\mathrm{m}},\ \mu^{\mathrm{M}}) \\ &= \sup_{\mu^{\mathrm{M}} \in \mathcal{M}_{\#}^{\mathrm{M}}} \inf_{v^{\mathrm{M}} \in \mathcal{W}^{\mathrm{M}}} \sum_{k=1}^{N} \inf_{v_k^{\mathrm{m}} \in \mathcal{W}_k^{\mathrm{m}}} L_k(v_k^{\mathrm{M}} + v_k^{\mathrm{m}},\ \mu_k^{\mathrm{M}}) \end{aligned}$$

where

$$L_k(v,\ \mu) = J_k(v) + C_k(v,\ \mu), \quad C_k(v,\ \mu) = -\int_{\partial\Omega_k} \mu v\, \mathrm{d}s \tag{40}$$

We define on each subdomain the homogenized functional

$$L_k^{\text{hom}}(v_k^{\text{M}}, \mu_k^{\text{M}}) = \inf_{v_k^{\text{m}} \in \mathcal{W}_k^{\text{m}}} L_k(v_k^{\text{M}} + v_k^{\text{m}}, \mu_k^{\text{M}}), \quad \forall (v_k^{\text{M}}, \mu_k^{\text{M}}) \in \mathcal{W}_k^{\text{M}} \times \mathcal{M}_k^{\text{M}} \tag{41}$$

Noting that

$$\mathcal{W}_{\#}^{\text{M}} \equiv \prod_{k=1}^{N} \mathcal{W}_k^{\text{M}}, \quad \mathcal{M}_{\#}^{\text{M}} \subset \prod_{k=1}^{N} \mathcal{M}_k^{\text{M}} \tag{42}$$

the saddle-point problem (3.19) finally takes the form

$$L(\tilde{w}, \lambda^{\text{M}}) = L^{\text{hom}}(w^{\text{M}}, \lambda^{\text{M}}) = \inf_{v^{\text{M}} \in \mathcal{W}^{\text{M}}} \sup_{\mu^{\text{M}} \in \mathcal{M}_{\#}^{\text{M}}} L^{\text{hom}}(v^{\text{M}}, \mu^{\text{M}}) \tag{43}$$

where

$$L^{\text{hom}}(v^{\text{M}}, \mu^{\text{M}}) = \sum_{k=1}^{N} L_k^{\text{hom}}(v_k^{\text{M}}, \mu_k^{\text{M}}), \quad \forall (v^{\text{M}}, \mu^{\text{M}}) \in \mathcal{W}^{\text{M}} \times \mathcal{M}_{\#}^{\text{M}} \tag{44}$$

REMARK. The problem (43) is well posed since the problem (34) is well posed and the fact that the direct sum condition (35) is imposed. On the contrary, the following saddle-point problem is not necessarily well-posed

$$L(w^{\text{M}}, \lambda^{\text{M}}) = \inf_{v^{\text{M}} \in \mathcal{W}^{\text{M}}} \sup_{\mu^{\text{M}} \in \mathcal{M}_{\#}^{\text{M}}} L(v^{\text{M}}, \mu^{\text{M}}) \tag{45}$$

The construction of the homogenized functional L^{hom} somehow ensures automatically the satisfaction of the LBB condition.

4. Finite element approximation

We now consider the practical case in which the subdomains Ω_k, $1 \leq k \leq N$ are meshed using finite elements, defining local finite element spaces $\mathcal{W}_k^h \subset \mathcal{W}_k \equiv H^1(\Omega_k)$. We assume that the meshes are conforming from subdomain to subdomain and that the periodicity condition may be exactly imposed. More precisely, the local finite element spaces $\mathcal{W}_k^h$, $1 \leq k \leq N$ are assumed to be such that

$$\mathcal{V}_{\#}^h = \{v \in C^0(\Omega): v_k \in \mathcal{W}_k^h, v(x) = v(x') \ \forall (x, x') \in \partial\Omega_{\#}\} \neq \{0\} \tag{46}$$

The primal reference problem (2.6) now reads

$$J(u_h) = \inf_{v \in \mathcal{V}_{\#}^h} J(v) \tag{47}$$

whereas the primal hybrid formulation (13) is now

$$L(w_h, \lambda_h) = \inf_{v \in \mathcal{W}^h} \sup_{\mu \in \mathcal{M}_{\#}} L(v, \mu) \tag{48}$$

where $\mathcal{W}^h$ is defined by

$$\mathcal{W}^h = \{w \in L^2(\Omega); w_k \in \mathcal{W}_k^h, 1 \leq k \leq N\} \tag{49}$$

We have the properties

- the saddle point problem (48) has a unique solution w_h. This solution belongs to $\mathcal{V}_{\#}^h$ and is equal to the solution u_h of (47); the solution λ_h is not necessarily unique.
- the following equality holds: $L(w_h, \lambda_h) = J(u_h)$.

As before, the goal is to compute approximate solutions $(\tilde{w}_h, \tilde{\lambda}_h)$ and $\tilde{u}_h$ providing lower and upper bound to the true energy i.e.

$$L(\tilde{w}_h, \tilde{\lambda}_h) \leqslant L(w_h, \lambda_h) = J(u_h) \leqslant J(\tilde{u}_h) \tag{50}$$

4.1. Upper bound

The upper bound is obtained by constructing a subspace $\tilde{\mathcal{V}}_{\neq}^h \subset \mathcal{V}_{\neq}^h$ and by defining $\tilde{u}_h$ as

$$J(\tilde{u}_h) = \inf_{v \in \tilde{\mathcal{V}}_{\neq}^h} J(v) \tag{51}$$

$\tilde{\mathcal{V}}_{\neq}^h$ is built as follows. On each subdomain Ω_k, we define the spaces $\mathcal{V}_k^{\mathrm{M},h}$ and $\mathcal{V}_k^{\mathrm{m},h}$ such that

$$\mathcal{V}_k^{\mathrm{M},h} = \{v \in \mathcal{W}_k^h : \exists v^{\mathrm{M}} \in \mathcal{V}^{\mathrm{M}} : v = \Pi_k v^{\mathrm{M}}\} \tag{52}$$

$$\mathcal{V}_k^{\mathrm{m},h} = \{v \in \mathcal{W}_k^h : v_k = 0 \text{ on } \partial\Omega_k\} \tag{53}$$

Π_k is a projection operator defined by

$$\Pi_k : \mathcal{V}_k^{\mathrm{M}} \to \mathcal{V}_k^{\mathrm{M},h} : u^{\mathrm{M}} \to u^{\mathrm{M},h} : u^{\mathrm{M},h} = u^{\mathrm{M}} \text{ on } \partial\Omega_k \text{ and } B_k(u^{\mathrm{M},h}, v) = B_k(u^{\mathrm{M}}, v) \forall\, v \in \mathcal{V}_k^{\mathrm{m},h}$$

If the condition $u^{\mathrm{M},h} = u^{\mathrm{M}}$ on $\partial\Omega_k$ does not hold, other types of projections may be considered. The corresponding global spaces are

$$\mathcal{V}_{\neq}^{\mathrm{M},h} = \{v \in \mathcal{V}_{\neq}^h : v_k \in \mathcal{V}_k^{\mathrm{M},h},\ 1 \leqslant k \leqslant N\} \cap C^0(\Omega) \tag{54}$$

$$\mathcal{V}_{\neq}^{\mathrm{m},h} = \{v \in \mathcal{V}_{\neq}^h : v_k \in \mathcal{V}_k^{\mathrm{m},h},\ 1 \leqslant k \leqslant N\} \tag{55}$$

$$\tilde{\mathcal{V}}_{\neq}^h = \{v = v^{\mathrm{M}} + v^{\mathrm{m}} : v^{\mathrm{M}} \in \mathcal{V}_{\neq}^{\mathrm{M},h},\ v^{\mathrm{m}} \in \mathcal{V}_{\neq}^{\mathrm{m},h}\} = \mathcal{V}_{\neq}^{\mathrm{M},h} + \mathcal{V}_{\neq}^{\mathrm{m},h} \tag{56}$$

and the inclusion $\tilde{\mathcal{V}}_{\neq}^h \subset \mathcal{V}_{\neq}^h$ holds. The practical computation of (51) follows the same step as in Section 3.

4.2. Lower bound

The lower bound in (50) is given by

$$L(\tilde{w}_h, \tilde{\lambda}_h) = \inf_{v \in \mathcal{W}} \sup_{\mu \in \tilde{\mathcal{M}}_{\neq}} L(v, \mu^{\mathrm{M}}) \tag{57}$$

where $\tilde{\mathcal{M}}_{\neq} = \mathcal{M}_{\neq}^{\mathrm{M}} \subset \mathcal{M}_{\neq}$ was defined in (32). Using the results in [12,13], the solution to the saddle-point problem (57) exists and is unique if the following condition is satisfied for all k, $1 \leqslant k \leqslant N$

$$\left\{\mu \in \mathcal{M}_k^{\mathrm{M}};\ \forall\, v \in \mathcal{W}_k^h \int_{\partial\Omega_k} \mu v \, \mathrm{d}s = 0\right\} = \{0\} \tag{58}$$

A way to ensure this condition in practice is to require that number of degrees of freedom charactering the temperature field on the boundary $\partial\Omega_k$ is strictly larger than the number of degrees of freedom characterizing the flux on $\partial\Omega_k$.

The practical computation of (57) follows the step detailed in Section 3. We work with the spaces $\mathcal{W}_k^{\mathrm{M},h}$ and $\mathcal{W}_k^{\mathrm{m},h}$ on each subdomain that must satisfy the direct sum condition

$$\mathcal{W}_k^h = \mathcal{W}_k^{\mathrm{M},h} \oplus \mathcal{W}_k^{\mathrm{m},h} \tag{59}$$

EXAMPLE. We take $\mathcal{W}_k^{\mathrm{M},h} = \mathcal{V}_k^{\mathrm{M},h}$ and

$$\mathcal{W}_k^{\mathrm{m},h} = \{v \in \mathcal{W}_k^h : \int_{\Omega_k} \nabla v \cdot \nabla v^{\mathrm{M}} \, \mathrm{d}x = 0 \quad \forall\, v^{\mathrm{M}} \in \mathcal{W}_k^{\mathrm{M},h},\ \int_{\Omega_k} v \, \mathrm{d}x = 0\} \tag{60}$$

5. Numerical experiments

We consider two 2-D numerical experiments. In both experiments, the domain is decomposed into quadrilateral subdomains over which a bilinear finite element type representation of the meso-scale temperature is used (in both primal and hybrid approach). For the hybrid approach, the micro temperature space is defined by (60) and the fluxes along the edges of the quadrilateral are constant.

5.1. RVE with circular inclusion

As a first simple problem, we consider the RVE shown in Fig. 4 containing 7 circular inclusions. The matrix and the inclusions are made of an isotropic heat conductor material whose conductivities are 1 and 100, respectively. The imposed temperature gradient is $\bar{\boldsymbol{\epsilon}} = (1, 0)$. The computation on the full mesh shown Fig. 5 gives the reference solution, Fig. 6. The reference homogenized heat conductivity in the x direction is $K = 1.4399$.

The RVE is decomposed into 9 subdomains along the lines shown Fig. 4. The computation needed for the conforming and hybrid approach is split among 9 processors of a cluster of Intel machines running Linux. The conforming and hybrid approaches give the solutions shown in Figs. 7 and 8, respectively. The bounds obtained on the homogenized conductivity are

$$K_- = 1.3903 \leqslant K = 1.4399 \leqslant K_+ = 1.4787 \tag{61}$$

whereas the Reuss and Voigt bounds are 1.09 and 18.92! The error on the average, $\langle K \rangle = (K_+ + K_-/2) = 1.4345$, is bounded by $\epsilon_K = (K_+ - K_-)/(K_+ + K_-) \simeq 3.08\%$.

In Figs. 9 and 10, we observe, as expected, that the 'conforming' temperature field is continuous whereas the 'hybrid' temperature field is not. On the other hand, the hybrid approach yields continuous heat fluxes but the conforming approach does not.

Concerning the quality of the micro-field, the energy error in the difference of the conforming and hybrid temperature field is

$$\epsilon^{\text{m}} = \left(\frac{\sum_{k=1}^{N} \|\tilde{u}_k - \tilde{w}_k\|^2_{E(\Omega_k)}}{\sum_{k=1}^{N} \|\tilde{w}_k\|^2_{E(\Omega_k)}} \right)^{1/2} = 24.03\% \tag{62}$$

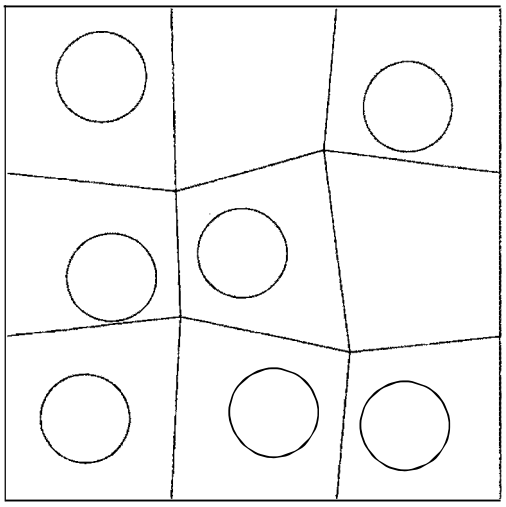

Fig. 4. RVE with circular inclusions: geometry of the problem and domain decomposition.

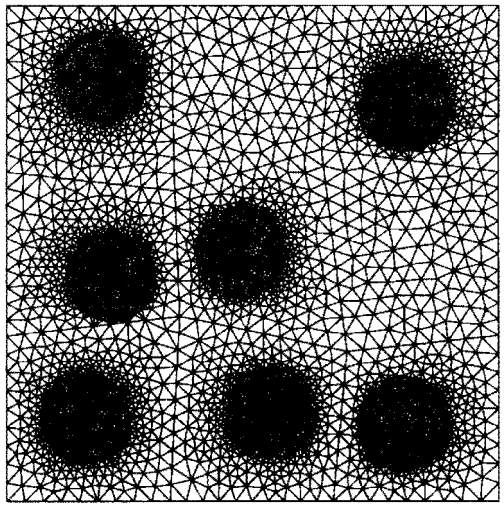

Fig. 5. The mesh defining the reference solution (4141 DOF).

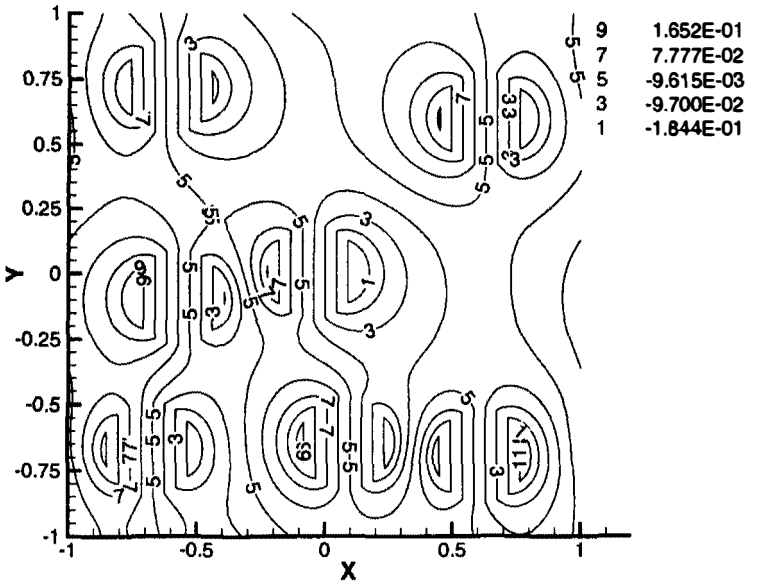

Fig. 6. Reference temperature field.

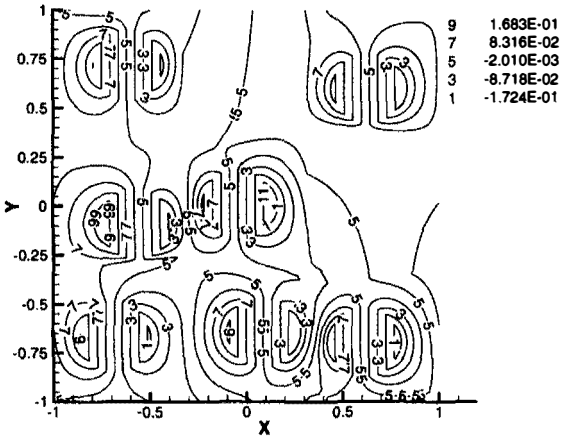

Fig. 7. Temperature field obtained by the conforming approach.

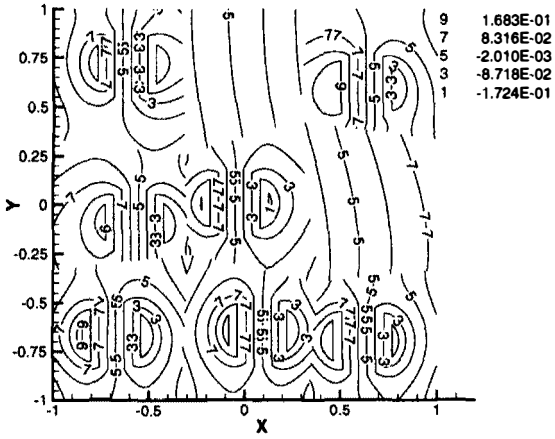

Fig. 8. Temperature field obtained by the hybrid approach.

The h index is omitted for the sake of simplicity of notation. The quantity $\epsilon^{\mathrm{m}}/2 = 12.02\%$, gives the exact error on the average in the two solutions:

$$\frac{\epsilon^{\mathrm{m}}}{2} = \epsilon^{\mathrm{m}}_{()} = \left(\frac{\sum_{k=1}^{N} \left\| \frac{\tilde{u}_k + \tilde{w}_k}{2} - \tilde{u} \right\|^2_{E(\Omega_k)}}{\sum_{k=1}^{N} \|\tilde{w}_k\|^2_{E(\Omega_k)}} \right)^{1/2} = 12.02\% \tag{63}$$

The proof may be found in [14] and uses the Prager–Synge hypercircle theorem [15].

The errors discussed above are modeling type errors. They come from simplified assumptions on the fluxes or temperature on the boundary of each subdomain. Table 1 gives the influence of the quality of the mesh on these modeling error. We observe a strong stability of the modeling errors when the mesh is refined.

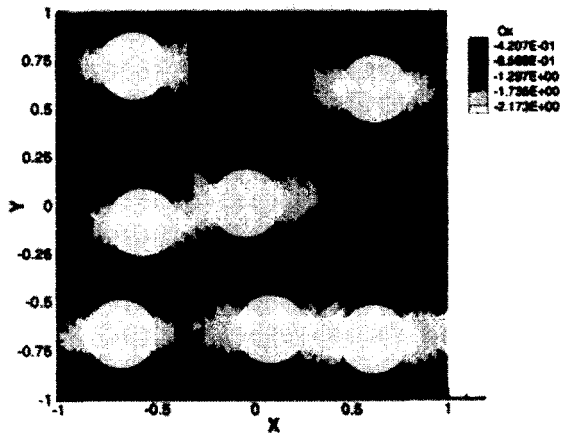

Fig. 9. x component of the heat flux obtained by the conforming approach.

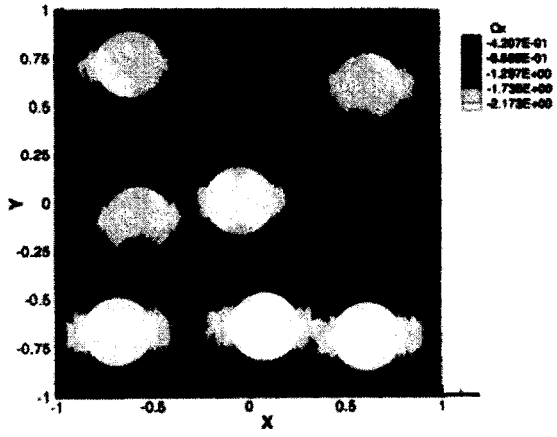

Fig. 10. x component of the heat flux obtained by the hybrid approach.

Table 1
Influence of the number of degrees of freedom in the mesh on the modeling errors ($\epsilon_{\langle\rangle} = (\langle K\rangle - K)/K$).

D.O.F.	$K_{\blacksquare}$	K	K_{+}	$\langle K\rangle$	ϵ_K (%)	$\epsilon_{\langle\rangle}$ (%)	ϵ^{m} (%)	$\epsilon^{m}_{\langle\rangle}$ (%)
188	1.5206	1.5782	1.5965	1.5585	2.44	−1.25	20.82	10.41
1018	1.3983	1.4502	1.4902	1.4443	3.18	−0.41	24.30	12.15
4141	1.3903	1.4399	1.4787	1.4345	3.08	−0.38	24.03	12.02
16376	1.3884	1.4374	1.4756	1.4320	3.05	−0.38	23.91	11.96
65507	1.3876	1.4362	1.4743	1.4309	3.03	−0.43	23.85	11.93

5.2. RVE with elliptic inclusions

The second example involves a more complex micro-structure, Fig. 11. The heat conductivity properties of the inclusions and the matrix are the same as in the previous example. The imposed temperature gradient is $\bar{\boldsymbol{\epsilon}} = (1, 0)$. The volume fraction of the inclusions is 3%. The mesh involves 276 875 DOF. The reference homogenized conductivity is $K = 1.1004$. The computation needed for the conforming and hybrid approaches is split over 14 processors. The bounds obtained are

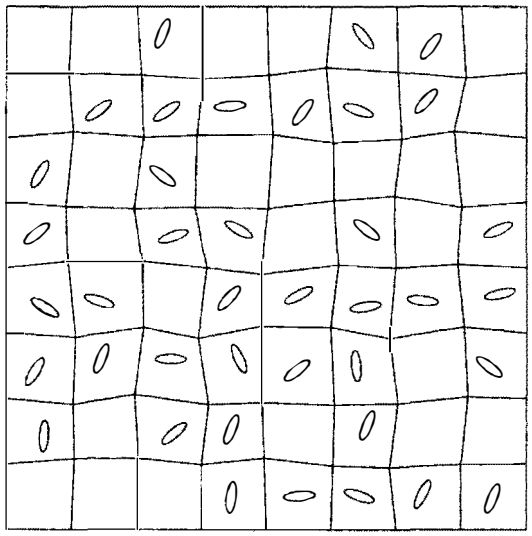

Fig. 11. RVE with elliptic inclusions: geometry of the problem and domain decomposition.

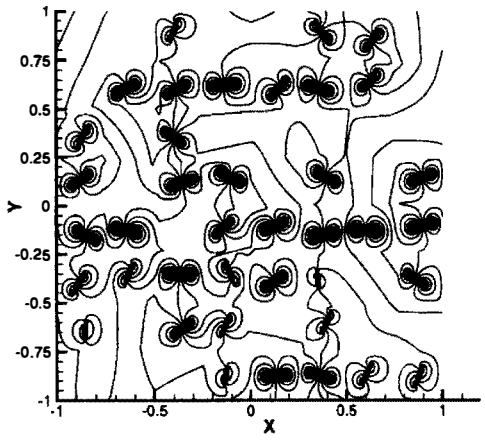

Fig. 12. Temperature field obtained by the conforming approach.

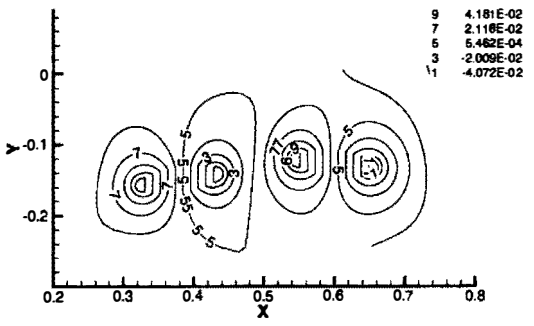

Fig. 13. Zoom on the temperature field obtained by the conforming approach.

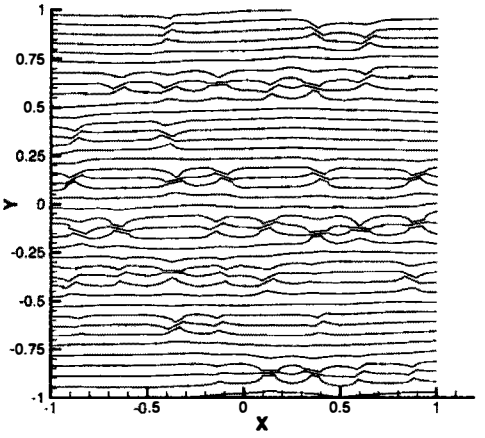

Fig. 14. Heat flux lines obtained by the hybrid approach.

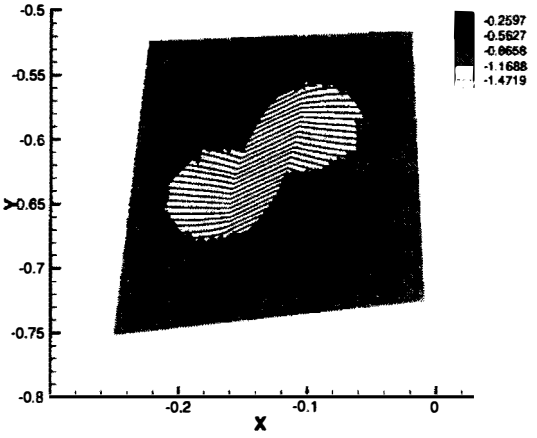

Fig. 15. Zoom in one subdomain: heat flux lines and x component of the heat flux.

$$K_- = 1.0971 \leqslant K = 1.1004 \leqslant K_+ = 1.1035 \tag{64}$$

whereas the Reuss and Voigt bounds are 1.03 and 3.97. The error on the average is bounded by $\epsilon_K = 0.29\%$ and the error on the average of the micro-field is $\epsilon_{\langle\rangle}^{\mathrm{m}} = 3.87\%$.

The Figs. 12 and 13 shows the iso-contour of the conforming temperature solution. Fig. 14 gives the heat fluxes lines (lines tangent to the heat flux at each point). They tend to concentrate in the inclusions. Fig. 15 shows the x component of the flux in one subdomain. The parallel heat flux lines in the inclusion indicates that the flux is constant in the inclusion.

6. Conclusion

Two simplified methods to analyze linear representative volume elements have been introduced. They are based on a two-scale decomposition of the sought approximate solution and yield upper and lower bounds to the exact homogenized properties. Due to this bound property, the a posteriori error estimation of the modeling error is straightforward. Moreover, the exact energy error associated to the average of the two approximate micro-fields may be computed using the Prager–Synge theorem.

The implementation of the methods uses finite elements for flexibility and parallel resources for speed. The interaction between the modeling error (the main concern in this paper) and the numerical errors should be

investigated in future work. In a first example, a strong stability of the modeling error with respect to the numerical error is observed.

Acknowledgments

N.M., J.T.O. and K.V. gratefully acknowledge the support of this work by the U.S. Office of Naval Research under Grant N00014-95-1-0401 and the National Science Foundation under grant ECS-9422707 and the Intel Corporation under Grant: Intel Grant Letter dated August 14, 1997 to The University of Texas at Austin. They are also grateful to Dr. Todd Arbogast for helpful discussions.

References

[1] E. Sanchez-Palencia, Non-homogeneous media and vibration theory, Lecture Notes in Physics (Springer-Verlag, 1980).
[2] P.M. Suquet, A simplified method for prediction of homogenized elastic properties of composites with a periodic structure, Compte-Rendus Acad. Sci. Paris, Série II, 311 (1990) 769–774.
[3] H. Moulinec and P.M. Suquet, A numerical method for computing the overall response of nonlinear composites with complex microstructure, Comput. Methods Appl. Mech. Engrg. 157 (1998) 69–94.
[4] S. Ghosh, K. Lee and S. Moorthy, Two scale analysis of heterogeneous elastic-plastic materials with asymptotic homogenization and voronoi cell finite element model, Comput. Methods Appl. Mech. Engrg. 132 (1996) 63–116.
[5] T.I. Zohdi, J.T. Oden and G.J. Rodin, Hierarchical modeling of heterogeneous bodies, Comput. Methods Appl. Mech. Engrg. 138(1–4) (1996) 273–298.
[6] J.T. Oden and T.I. Zohdi, Analysis and adaptive modeling of highly heterogeneous elastic structures, Comput. Methods Appl. Mech. Engrg. 148(3–4) (1997) 367–391.
[7] N. Moës, J.T. Oden and T.I. Zohdi, Investigation of the interactions between the numerical and the modeling errors in the homogenized dirichlet projection method. Comput. Methods Appl. Mech. Engrg., 158 (1998) 79–101.
[8] T. Arbogast, Private communication.
[9] P.M. Suquet, Elements of homogenization for inelastic solid mechanics, in: Sanchez-Palencia and Zaoui [16] 194–275.
[10] E. Jones, A generalization of the direct-stiffness method of structural analysis, AIAA J. 2 (1964) 821–826.
[11] T.H.H. Pian and P. Tong, The basis of finite element methods for solid continua. Int. J. for Num. Methods in Engrg. 1 (1969) 3–28 .
[12] P.-A. Raviart and J.M. Thomas, Primal hybrid finite element methods for 2nd order elliptic equations, Math. Comput. 31(138) (1977) 391–413.
[13] I. Babuska, J.T. Oden and J.D. Lee, Mixed-hybrid finite element approximations of second-order elliptic boundary value problems, Comput. Methods Appl. Mech. Engrg. 11 (1977) 175–206.
[14] N. Moës, J.T. Oden and K. Vemaganti, A two-scale strategy and a posteriori error estimation for modeling heterogeneous structures, in: P. Ladevèze and J.T. Oden, eds., Adavances in Adaptive Computational Methods in Mechanics, Studies Appl. Mechanics #47 (Elsevier Publication, 1998) 115–135.
[15] W. Prager and J.L. Synge, Approximation in elasticity based on the concept of functions space, Quart. Appl. Math. 5 (1947) 261–269.
[16] E. Sanchez-Palencia and A. Zaoui, eds., Lecture Notes in Physics (Springer-Verlag, 1985).